Vortex-sound Generated Pressure Oscillations Simulation in Internal Flow by means of Q-1D Model

V. Ferretti⋆ and B. Favini⋆ and E. Cavallini⋆ and F. Serraglia⋆⋆ and M. Di Giacinto⋆

⋆Sapienza University of Rome, Italy
Dipartimento di Ingegneria Meccanica e Aerospaziale, via Eudossiana 18, I-00184 Rome, Italy
⋆⋆VEGA IPT ESA/ESRIN, Frascati (Rome), Italy

Abstract

The quasi-steady operative condition of large solid rocket motors could exhibit the presence of sustained pressure and thrust oscillations, at a frequency close to the acoustical fundamental, or one of its multiple, of their motor chamber. The phenomenon occurs because of a coupling between shear layer instabilities, with vorticity generation and convection, and acoustical feedback resulting from destroy of vorticity by some geometrical features of combustion chamber, as port area variations or nozzle walls.

In the present work the analysis of solid propellant rocket motor aero-acoustic phenomena is obtained by applying a quasi-onedimensional model. The proposed model is derived formally from the Euler conservation laws. The model, implemented into a code named AGAR (Aerodinamically Generated Acoustic Resonance), is applied to a cold flow in a axisymmetric combustor as test case.

1. Introduction

A certain number of large solid rocket motor (SRM), such as US Space Shuttle SRM[1], Ariane 5 P230 SRM [2], Titan SRM and the five-segment test motor ETM-3, exhibit sustained pressure, and then thrust, oscillations during their whole operative life. Generally characterized by a frequency close to the acoustic modes of the combustion chamber, these oscillations can couple with the launcher structural modes, involving structural failures, interferences and payload damages. Furthermore, thrust oscillations can affect the motor performance and can result in guidance complications.

The pressure oscillations result from the complex feedback mechanism fed by vortex shedding and acoustic waves, and are due to the coupling between *fluid-dynamics instabilities* and *acoustic resonant modes*. The first description of the *resonant oscillation* has been developed by Rossiter[3], in a different contest with respect to the internal ballistic, that describes the aeroacoustic coupling as a feedback loop (fig.1). The hydrodynamic instability of the shear flow generates vortical structure; three kinds of vortex shedding phenomena can be identified in a SRM: parietal, obstacle and corner vortex shedding. Once detached, these structures are convected by the flow and interacts with each obstacle in the combustion chamber (inhibitor rings, annular restrictors, nozzle,...). Each interaction determines an acoustic field excitation and a possible acoustical triggering of shear flow instability.

The vortex shedding process is related to the stand-off distance (l_i) and it is characterized by the frequency f_{vs}. The acoustics is instead related to the combustion chamber length (L) and it is characterized by the frequency f_a. When the two loops are coupled, and the vortex shedding frequency is synchronised with the chamber acoustic modes ($f_{vs} = f_a$), the resonant coupling occurs, leading to self-sustained coupled-mode oscillations.

Several model have been proposed for the aeroacoustic modeling. Among the others it is worth to mention the acoustic balance technique, developed by Culick [4], a linear stability analysis of the chamber acoustic modes, and Flandro's method, a complex linear theory based on the hydrodynamic stability analysis, represents the most important method used for the stability analysis [5].

Due to the geometrical configuration of the combustion chamber of a SRM, the longitudinal modes are the most important, so that the transverse modes can be neglected and a one-dimensional model can be considered. Matveev derived a one-dimensional model, based on a system of ordinary differential equation, that describes the acoustic modes excitation accounting for the acoustic feedback on the vortex shedding process [6, 7]. Jou and Menon proposed a one-dimensional model that describes the interaction between the acoustic wave and the vortical disturbance and provides a method for the approximative evaluation of the coupled mode frequencies [8, 9].

In the present work a quasi-onedimensional model for the simulation of the flow time evolution in SRMs is presented. The analysis of the obtained pressure oscillations allows to characterize these oscillations as far as it concerns both amplitude and frequency. The simulation of a cold flow in an axisymmetric ramjet combustor is here performed and the same test case proposed by Jou and Menon is analyzed. A comparison with their result is also provided.

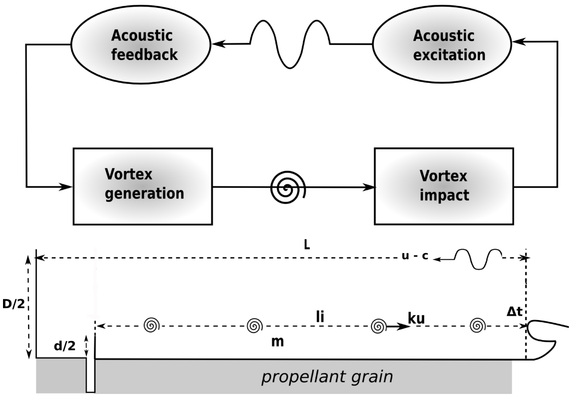

Figure 1: Aeroacoustic coupling.

2. Vortex-sound quasi-one dimensional model

A quasi-one dimensional model for the simulation of the flow time evolution in solid rocket motors is here presented. The analysis of the obtained pressure time evolution allows to characterize the pressure oscillations as far as it concerns both amplitude and frequency. A complete description of the model can be found in [10, 11, 12].

It uses an unsteady Eulerian model with mass, momentum and energy addition and a geometrical evolution both in space and time. Two phase flow effects are neglected and a mixture of non reacting perfect gases is considered. The thermophysical properties of the mixture of ideal gases are variable in space and time; they are evaluated using a thermodynamic standard model for mixtures. Further, the grain combustion reactions are supposed to occur in an ideal thin layer on the grain propellant surface and the mass produced by the propellant combustion is supposed to be added without axial momentum. The effects related to combustion instability are also not considered.

The governing equation that has to be considered are the mass, momentum and energy conservation equation and the vorticity equation. The three-dimensional equations, expressed in cylindrical coordinates for an axysimmetric flow and averaged on the normal sections, can be expressed in a quasi-one-dimensional form as follows:

$$
\left\{
\begin{array}{lll}
\dfrac{\partial\left(\rho_i A_p\right)}{\partial t} + \dfrac{\partial\left(\rho_i u_x A_p\right)}{\partial x} & = r_b P_b \rho_p + \dot{m}_s + \dot{m}_{vs} & \text{for } i = 1,\ldots,6 \\[2ex]
\dfrac{\partial\left(\rho u_x A_p\right)}{\partial t} + \dfrac{\partial\left[\left(\rho u_x^2 + p\right) A_p\right]}{\partial x} - p\dfrac{\partial A_p}{\partial x} & = \dot{q}_{vs} & \\[2ex]
\dfrac{\partial\left(\rho e A_p\right)}{\partial t} + \dfrac{\partial\left[(\rho e + p)\, u A_p\right]}{\partial x} & = r_b P_b \rho_p H_f + \dot{m}_s H_s + \dot{e}_{vs} & \\[2ex]
\dfrac{\partial(\rho\omega_\theta A_p)}{\partial t} + \dfrac{\partial(\rho\omega_\theta u_x A_p)}{\partial x} + \displaystyle\int_S \rho\omega_\theta \dfrac{\partial u_x}{\partial x}\, dS & = -\displaystyle\int_S \dfrac{\partial(\rho\omega_\theta u_r)}{\partial r}\, dS - \int_S \rho\omega_\theta \dfrac{u_r}{r}\, dS\, \dfrac{u_r}{r}\, dS - \int_S \rho\omega_\theta \dfrac{\partial u_r}{\partial r}\, dS & \\[2ex]
 & = S_{\omega 1} + S_{\omega 2} + S_{\omega 3} &
\end{array}
\right. \tag{1}
$$

where A_p represents the combustion chamber port area, r_b the propellant burning rate, P_b the combustion perimeter, ρ_p the propellant density, $\dot{m}_s$ the cavity mass flow rate addition per unit length, H_f is the grain combustion products enthalpy per unit mass and H_s is the cavity gases enthalpy per unit mass. The evolution of the cross-sectional port area evolution A_p does not include slots and submergence regions; their presence is treated by the source terms in the mass and energy equations.

The $\dot{m}_{vs}$, $\dot{q}_{vs}$ and $\dot{e}_{vs}$ are the source terms that describes the excitation of the acoustic field by vortex shedding phenomenon.

The source terms in the vorticity equation represent the radial addition, $S_{\omega 1}$, the deformation contribution, $S_{\omega 2}$, and the comprimibility effects, $S_{\omega 3}$; comprimibility effects are also described by the term $\int_S \rho\omega_\theta \frac{\partial u_x}{\partial x}\, dS$. The radial term in $S_{\omega 1}$, $S_{\omega 2}$ and $S_{\omega 3}$ have to be properly modeled for the closure of the model.

If the deformation and the comprimibility effects are not considered, the terms $S_{\omega 2}$, $S_{\omega 3}$ and $\int_S \rho\omega_\theta \frac{\partial u_x}{\partial x}\, dS$ are neglected. The only term that remains is the radial addition term $S_{\omega 1}$, that is here modeled as the addition due to the presence of a corner. $S_{\omega 1}$ is expressed as:

$$S_{\omega 1} = \rho \frac{d\Gamma}{dt} \tag{2}$$

that exists only in correspondence of the corner where the vortex generation takes place. Obstacle and parietal vortex shedding phenomena are then not described by this model. With the assumptions just presented, the considered vorticity equation is:

$$\frac{\partial(\rho\omega_\theta A_p)}{\partial t} + \frac{\partial(\rho\omega_\theta u_x A_p)}{\partial x} = \rho \frac{d\Gamma}{dt} \tag{3}$$

In order to simplify the adopted notation, indicated with u and ω respectively the u_x and the ω_θ component, the Ω variable is introduced:

$$\Omega = \rho\omega A_p \tag{4}$$

Ω characterizes the vorticity field. The eq. 3 can be rewritten in function of the Ω variable as:

$$\frac{\partial\, \Omega}{\partial t} + \frac{\partial\, (\Omega\, u)}{\partial x} = \rho\, \dot{\Gamma} \tag{5}$$

The vortex shedding phenomenon can be excited by the acoustic field. This influence is described by the definition of the vortex properties as a function of time varying flow conditions. If the velocity at the outer edge of the boundary layer is assumed composed by the mean flow velocity $\overline{u}$ and acoustic component $u^{'}$, the rate of circulation production can be approximated by:

$$\dot{\Gamma} = \frac{d\Gamma}{dt} = u^2(t) \tag{6}$$

The rate of variation of the circulation, u_Γ, can be expressed as:

$$u_\Gamma = k_\Gamma\, u^2(t) \tag{7}$$

where k_Γ is a calibration parameter. The dependence on the flow velocity $u(t)$ underlines the acoustic influence on the vortex shedding.

As for the vortex creation and growth, also the detachment criterion is developed as a function of time varying flow conditions. The dependence from the local pressure evolution $p(t)$ at the shedding point underlines the role of the acoustic feedback on vortex shedding dynamics. The vortex separation is imposed each time the $p(t)$ at the detachment point verifies the following conditions:

$$\frac{d^2 p}{dt^2} = 0 \tag{8}$$

$$\frac{dp}{dt} \Rightarrow \textit{local minimum} \tag{9}$$

that corresponds to impose the detachment each time the $p(t)$ evolution presents a descendent node (positive velocity antinode).

The excitement of the acoustic field, due to the vortex interaction/impingement with an obstacle, is described by the introduction of source terms in the Euler equations ($\dot{m}_{vs}$, $\dot{q}_{vs}$ and $\dot{e}_{vs}$ in eq. 1). The mass source term $\dot{m}_{vs}$ is assumed to be zero, so that the vortex impingement only generates momentum and energy source terms. A phenomenological description, combined with a dimensional analysis, determines the following expressions:

$$\dot{m}_{vs,i} = 0 \tag{10}$$

$$\dot{q}_{vs} = \Omega \frac{u}{A_p}\left(\frac{dA_p}{dx}\right)^2 \tag{11}$$

$$\dot{e}_{vs} = \rho u \dot{q}_{vs} = \frac{\rho\Omega}{A_p}\left(u\frac{dA_p}{dx}\right)^2 \tag{12}$$

The sound generation is active each time a vortex interacts with a geometrical variation. The influence of the vortex intensity is represented by the Ω dependence, while the effect of the angle between the vectors is described by the $\frac{dA_p}{dx}$ term.

3. Internal Ballistic quasi-one dimensional model AGAR

AGAR model is composed by the following submodels: a gasdynamic model, a model to evaluate the combustion rate of ignited propellant grain to evaluate the mass addition from burning surface, a model to determine the evolution of chamber geometry and an aeroacoustic model.

The gasdynamic model is the *SPINBALL* (Solid Propellant rocket motor INternal BALListics) model, created for the analysis of solid rocket motor internal ballistics and already completely developed; a detailed description can be found in [13]. An unsteady quasi-one-dimensional Eulerian model is used, with mass, momentum and energy addition and a geometrical evolution both in space and time. The “six-gases model” that is used allows the analysis of thermophysical properties variable in space and time, and it is not interested in the spatial time evolution of the single mixture gas (igniter, pressurising gas or propellant combustion products) [14]. The governing equation are discretized by a Godunov-type scheme, accurate at first or second order in space and time. The main model is completed by different submodels (e.g.: cavity model, heat transfer model).

The grain burnback analysis is the study of the burning surface evolution with time. The used grain burnback model is the 3D numerical model *GREG* (Grain REGression); a complete description can be found in [13]. It makes available the all geometrical parameters required for the solution of the internal ballistics. The use of a 3D model allows the analysis of complex 3D grain shapes (i.e: finocyl grains), also for 0-D or 1-D flow models. The model provides the all Q-1D geometrical parameters that are required, the space and time evolution of port area, cavities, burn and wet perimeter. It has to be coupled with the unsteady flowfield model and an off-line coupling is realized between the gasdynamic and the grain burnback model. Before the execution of the numerical simulation, it evaluates the grain burning surface, obtained with the assumption of a constant burning rate. During the simulation, gasdynamic model uses the data contained in these tables with an interpolation procedure.

The adopted aeroacoustic model is composed by the following submodels: a model to determine the vortex dynamics (creation, growth, convection and destruction), a model to evaluate the acoustic field excitation by vortex shedding phenomenon and a model to estimate the acoustically forced vortex generation. A quasi-onedimensional equation described the vorticity convection by the flow and the acoustic mode excitation by vortex impingement is modeled with the introduction of source terms in the gasdynamic model. A detailed description can be found in [10, 11, 12].

4. Numerical simulation of oscillatory cold flows

A simulation performed with cold flow allows the description of pure aeroacoustic coupling without any effect related to combustion instabilities. The simulation of a cold flow in an axisymmetric ramjet combustor is here performed. Jou and Menon [8, 9] proposed a cold flow simulation as test case for their one-dimensional model. The same test case is here provided and a comparison with their result is presented.

The considered geometrical configuration can be seen in fig. 2. A uniform grid of 400 cell is used; the step is located at cell 143, while the throat is at cell 354. The step is discretized by 20 cells and it is characterized by a height/length ratio of $h/l = 2.268$. While the throat and exit area values of the nozzle are correctly assumed, the nozzle profile is arbitrarily reconstructed.

The used initial conditions are that of a quiescent flow at stagnation conditions.

Subsonic inflow conditions are imposed at the inlet entrance ($M_{in} = 0.32$) and the inlet flow is assumed at an imposed total pressure and temperature. While the total temperature value is determined using the system acoustic frequency, the pressure value is arbitrarily chosen. The imposed value are $T_0 = 290K$ and $P_0 = 10\ bar$.

A seal, located in the nozzle throat section, protects the system, assumed at the total pressure value, from the external ambient, assumed at the atmospheric pressure. After the seal breaking, the throat section impulsively reaches the sonic condition. Once the system reaches the stationary conditions, the vortex shedding is activated. The only vortex shedding that is considered is the corner vortex shedding, corresponding to step position.

The assumptions used to complete the data set presented by Jou and Menon (e.g: nozzle geometry, total pressure value) do not modify the qualitative description of the considered phenomena but only affect the quantitative aspects.

A comparison with the oscillation amplitude obtained by Jou and Menon allows to determine the value of the k_Γ parameter.

The analysis of the frequency content of a signal is performed with the Fast Fourier Transform.

The pressure oscillations are analysed at the base of the step and at the nozzle throat section. The frequency content of the vortical field is obtained by analysing the Ω variable fluctuations; these oscillations are analysed both at the vortex detachment point and at the nozzle throat section. The vorticity and pressure oscillations evaluated in different sections of the system permit to obtain informations about the dynamics in the combustion chamber. A comparison can be done between Jou and Menon's results and the pressure oscillation at the nozzle throat section and the vorticity fluctuation at the vortex detachment point.

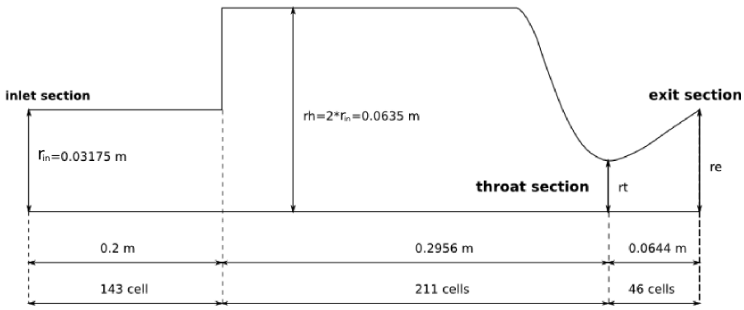

Figure 2: Test case geometry.

The pressure, velocity, speed of sound and Mach number distributions can be seen in fig. 3. At cell $\sim$ 230 a pressure node can be noted, corresponding to a velocity, and Mach, antinode.

The presence of a vortex corresponds to a local maximum in the vorticity (Ω) distribution; in fig. 4 six vortices can be noted.

A resonant condition corresponds to the detachment of vortices with the same frequency and with the same intensity. In this condition the vorticity distribution is characterized by a "regular" envelopment. The "non-regular" behaviour underlined in fig. 4 exhibits a non resonant configuration.

This is also reflected by the pressure and the velocity time evolution at the vortex detachment cell. The vortex detachment almost occurs at pressure negative antinode and positive velocity antinode.

The vortex shedding separation criterion can be seen in fig. 5, where the first and the second time pressure can be seen and where the red lines corresponds to the separation of a vortex. In this case the separation occurs in correspondence of velocity local maximum, in agreement with literature observations, and of pressure local minimum.

The pressure oscillations, at the base of the step and at the nozzle throat area, and the vorticity (Ω) oscillations can be seen in fig. 6. Both the pressure and the vorticity exhibit a damping effect with the flow motion towards the nozzle. Also the frequency content changes along the axis, showing that acoustics and vortex shedding interacts along the combustion chamber.

The frequency spectrum of each analysed signal can be seen in fig. 7. The frequency peaks obtained by Jou and Menon's simulation are indicated by the black vertical line.

The pressure at the base of the step exhibits two acoustic peaks, the first mode frequency at $\sim$ 650 Hz and the second mode peak at $\sim$ 1300 Hz. Two other peaks, $\sim$ 330 and $\sim$ 980 Hz, are related to the vortex shedding. The acoustic peaks remain the fundamental components for the pressure spectrum both at the base of the step and at the nozzle throat, where the vortex shedding frequencies are highly damped.

The vorticity (Ω) spectrum at the detachment point has its major contribution in the first acoustic mode; are contribution are the second acoustic mode and the two peaks related to the vortex shedding. At the throat section the acoustic frequency are almost completely damped and only remains the $\sim$ 330 Hz peak of the vortex shedding.

This behaviour shows that moving towards the nozzle throat, the acoustics and the vortex shedding phenomenon tend to decouple. While at the step position each signal shows the frequencies related to both the phenomena, at the nozzle section the vorticity field exhibits the only shedding frequency, while the pressure shows almost the only first acoustic mode contribution. The existence of these two separated frequency underlines the non resonant configuration of this test case (a resonant configuration is characterized by a single frequency peak related to both the phenomena).

Comments The phenomenological descriptions and the results that has been obtained are in agreement with the analysis performed by Jou and Menon. Some quantitative difference is related to the assumption used in order to complete the data set (i.e: the inlet pressure value). The model is able to describe the characteristics of both acoustics and vortex shedding.

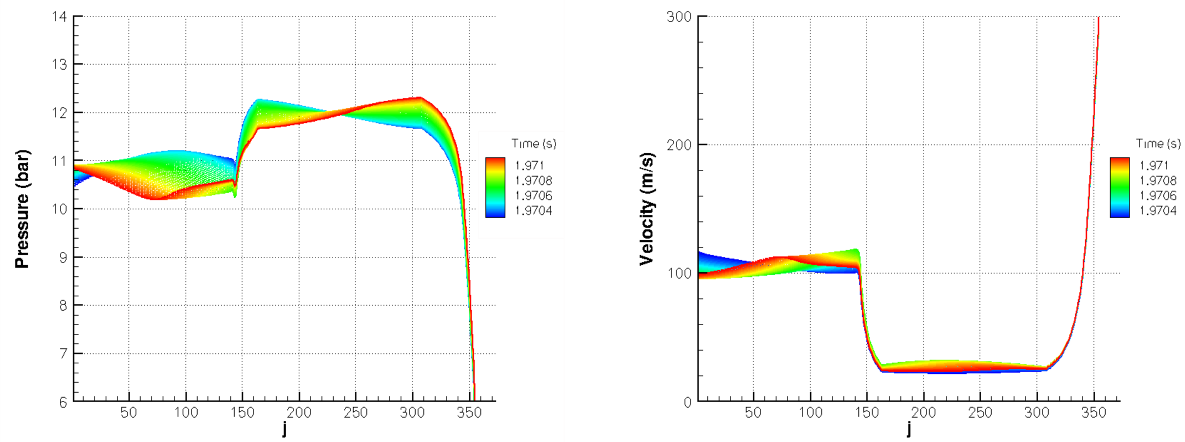

(a) Pressure (b) Velocity

Figure 3: M_{in} = 0.32 - Pressure and velocity distribution.

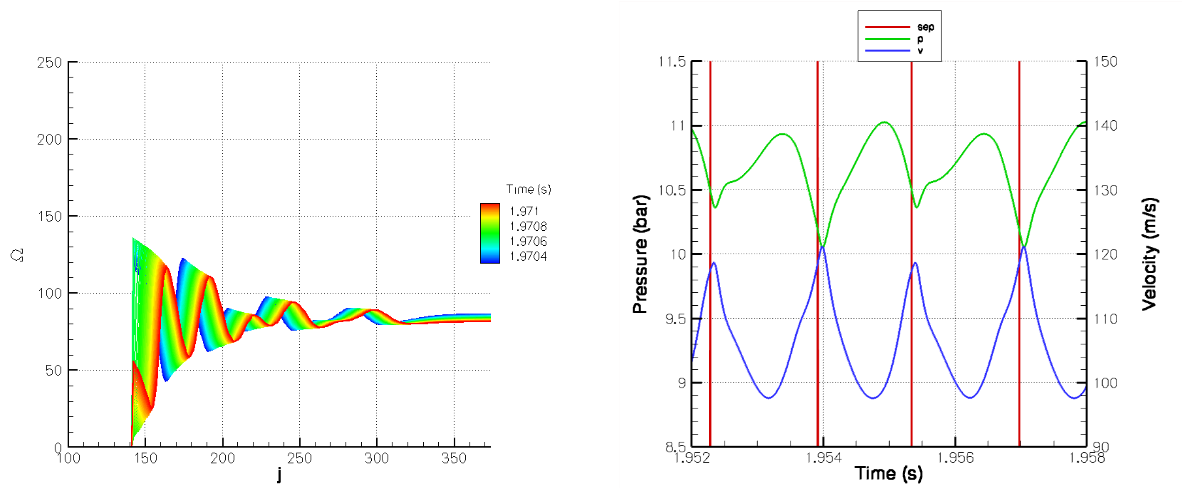

(a) Pressure time derivatives (b) Pressure and velocity

Figure 4: M_{in} = 0.32 - Vorticity (Ω) distribution and vortex detachment condition at vortex detachment cell.

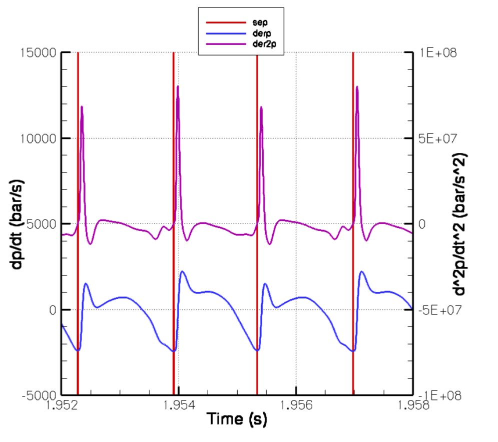

Figure 5: M_{in} = 0.32 - Vortex detachment condition at vortex detachment cell.

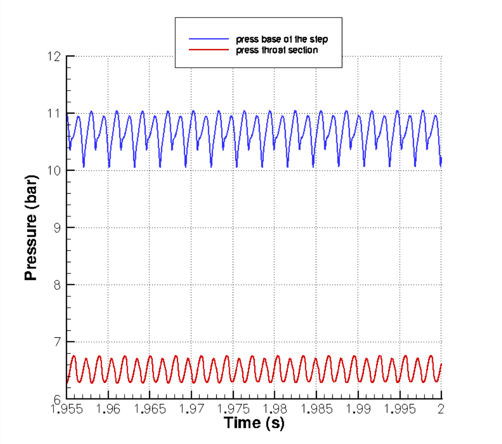

(a) Pressure

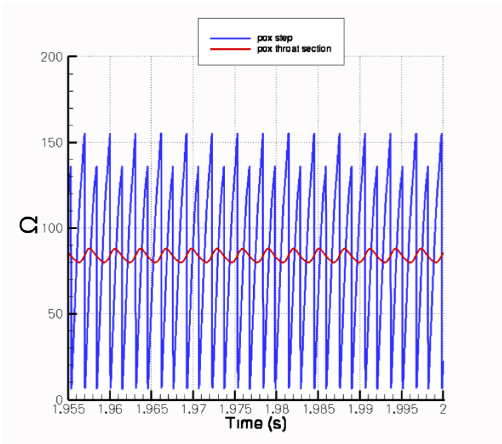

(b) Vorticity (Ω)

Figure 6: M_{in} = 0.32 - Pressure and vorticity (Ω) time evolution.

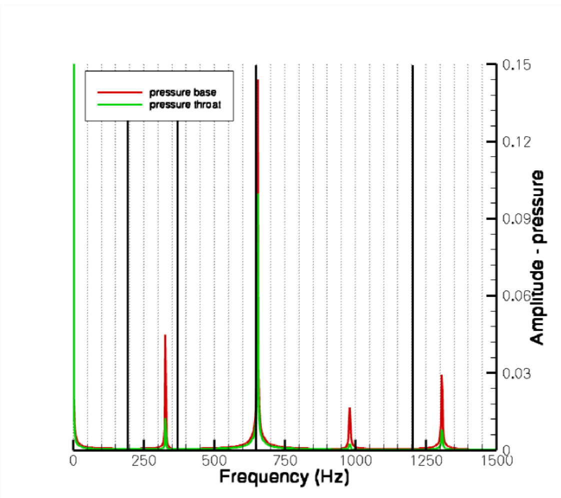

(a) Pressure spectrum.

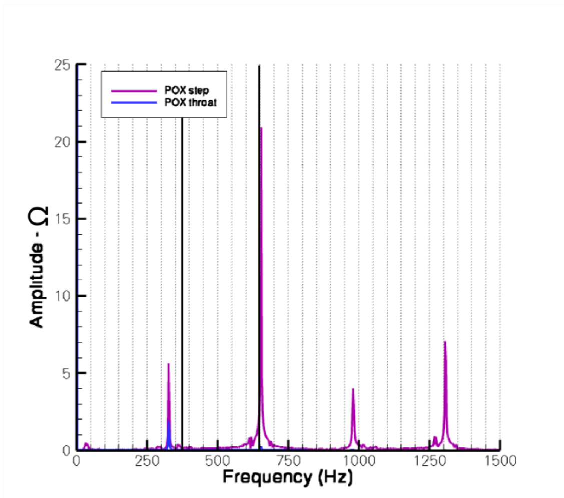

(b) Vorticity (Ω) spectrum zoom.

Figure 7: M_{in} = 0.32 - Pressure and vorticity (Ω) spectrum.

5. Inlet Mach number effect

In order to describe and to analyse the possible coupling between the acoustics and the vortex shedding phenomena, different inlet Mach number are considered. The same values assumed by Jou and Menon are considered, $M_{in} = 0.32, 0.44$; other test case that are provided are $M_{in} = 0.7, 0.55, 0.38, 0.25$.

Each different inlet condition is obtained modifying the area ratio of the system geometry, maintaining a constant value of the nozzle throat section; the considered geometries can be seen in fig. 8. The consequent dA/dx variations, affecting the model source term (eq. 10), for each case determine different oscillation amplitudes.

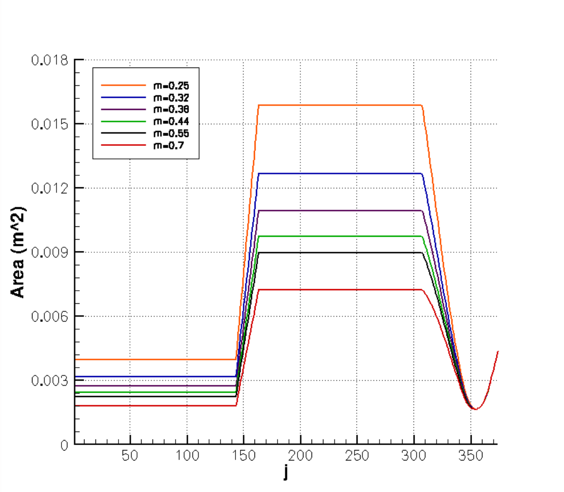

Figure 8: M_{in} effects - Test cases geometrical configuration.

The analysis of subsequent configuration, from $M_{in} = 0.7$ to $M_{in} = 0.25$, can be also interpreted in relation to a solid rocket motor. The functioning of a SRM is characterized by the regression of the combustion surface, related to an increasing of the port area and to a decreasing of the flow Mach number. As can be seen in fig. 8, the decrease of the M_{in} corresponds to geometrical configurations characterized by increasing port area. The analysis of each considered test case, from $M_{in} = 0.7$ to $M_{in} = 0.25$, can be seen as a sequence of following steady state describing the functioning of a SRM. If this idea is followed, the analysis and the comparison of each configuration describes the possible shift of the system towards and from the resonant condition during the motor functioning.

The pressure and velocity distributions obtained for each test case can be seen in fig. 9, 10. The pressure distribution shows a downstream moving of the node position (velocity antinode) related to the increase of the M_{in}. The resonant cases attain mean pressure values higher than that reached in non resonant conditions. The mean flow velocity increases with the M_{in}.

The vorticity (Ω) distribution is showed in fig. 11. The non regular envelopment of M_{in}=0.25, 0.7 describes a non resonant configuration (detachment of vortices of variable intensity); the other cases exhibit a resonant condition.

The number of detached vortices, corresponding to the number of relative maxima, is reduced by the increase of the M_{in} number. A velocity increase, involving an increase of the vortex convection velocity, requires a lower number of vortices in order to obtain the same frequency value. From the six vortices of the M_{in}=0.25 and M_{in}=0.38 cases, this number decrease to the five for M_{in}=0.44 and M_{in}=0.7 and to four for M_{in}=0.55.

The M_{in} increase determines a slight shift of the resonance frequency.

As shown in fig. 12, the imposed detachment conditions do not necessarily identify a pressure descending node. The shedding occurs at pressure local minimum (velocity local maximum), in agreement with literature observations. Also in fig. 12 can be distinguished the resonant (M_{in}=0.38, 0.44, 0.55) and non resonant (M_{in}=0.25, 0.7) cases.

The frequency content of the pressure and vorticity (Ω) fluctuations can be seen in fig. 13.

The simulation for M_{in}=0.38, 0.44, 0.55 exhibit resonant coupling conditions, as shown by both pressure and the vorticity spectra. The only frequencies that can be noted in the pressure spectrum correspond to the first (~ 590-660 Hz) and to the second (~ 1180-1330 Hz) acoustic mode. The resonant frequency slightly decreases with the M_{in} increase; this shift is greater for the second than for the first acoustic mode. The vorticity spectrum evaluated at the step exhibit only two frequency peaks corresponding to the acoustic modes; at the nozzle throat section the only first mode can be seen. The existence of a single frequency that describes both the acoustics and the vortex shedding underlines the resonance condition.

For the pressure spectrum of M_{in}=0.25, 0.38, 0.44, 0.55, the first acoustic mode remains the dominant contribution also at the nozzle throat section. For M_{in}=0.55, the second mode increases its contribution with respect to the base of the step section. This effect is amplified for M_{in}=0.7, that presents an energy passage from the first to the second mode, that becomes the dominant contribution at the nozzle.

The M_{in}=0.7 case shows an increasing importance of the vortex shedding frequencies (~ 130 and ~ 1050 Hz) and a non regular behaviour of the vorticity distribution (fig. 11). These condition can be seen as the indication that the system is moving away from resonant configuration.

While the resonant cases exhibit the only resonant frequencies, the non resonant cases (M_{in}=0.25, 0.32, 0.7) show different frequency components related to the vortex shedding phenomenon (~ 330 and ~ 980 Hz). These frequencies are visible in the pressure spectrum (both at the base of the step and at the nozzle throat) and in the vortical field; while the vorticity spectrum at the step also shows the acoustic component, at the nozzle throat the ~ 330 Hz is the only visible frequency, underlining a decoupling of the two analysed phenomenon in the combustion chamber.

Comments The adopted model correctly describes the main phenomena characterising the acoustic resonance and the system adjustment to resonance conditions. The performed analysis for the effect of M_{in} increase shows that the system moves from a non-resonant condition (M_{in}=0.25, 0.32) to a resonant one (M_{in}=0.38, 0.44, 0.55) and then it moves away from it (M_{in}=0.7).

While these simulations show a resonant configuration for M_{in}=0.44, Jou and Menon's results exhibit a movement towards resonant condition, but this configuration is not reached.

6. Concluding Remarks

In the present work a quasi-onedimensional model for the simulation of the flow time evolution in SRMs is presented. The analysis of the obtained pressure oscillations allows to characterize these oscillations as far as it concerns both amplitude and frequency.

The model is able to describe the fundamental characteristics of both acoustics and vortex shedding phenomenon, both in case of acoustic coupling and non resonant condition.

The test case that has been here presented is the same proposed by Jou and Menon, the simulation of a cold flow in an axisymmetric ramjet combustor. The obtained results are in good agreement with their study. Some quantitative difference is related to the assumptions introduced to complete the data set and to perform the simulation.

The analysis of configurations characterized by decreasing inlet Mach number and increasing port area can be seen as a sequence of following steady state describing the functioning of a SRM. The model describes resonant and non resonant conditions, and the system adjustment to resonance conditions.

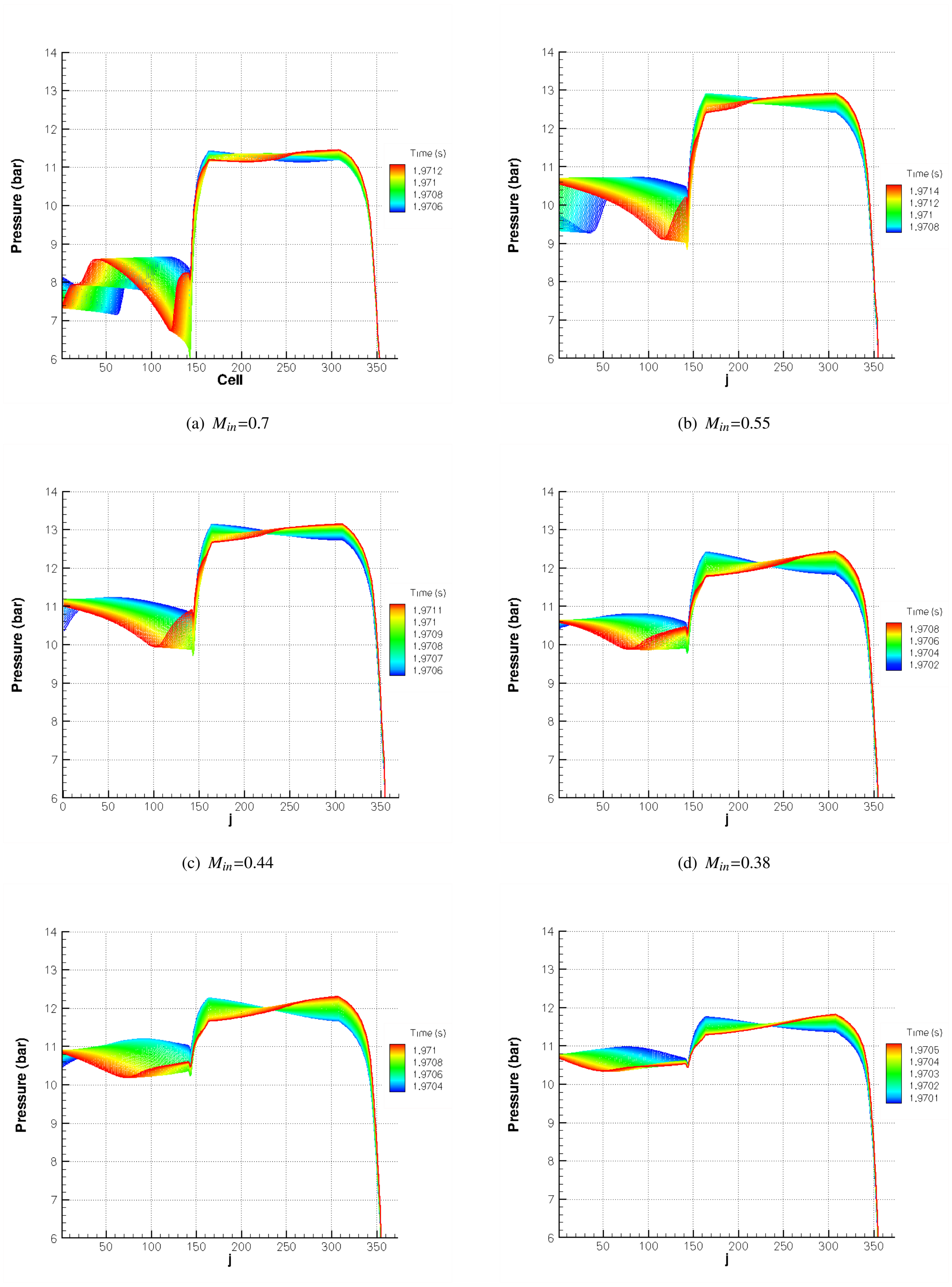

(a) M_{in}=0.7

(b) M_{in}=0.55

(c) M_{in}=0.44

(d) M_{in}=0.38

(e) M_{in}=0.32

(f) M_{in}=0.25

Figure 9: M_{in} effects - Pressure combustion chamber distribution.

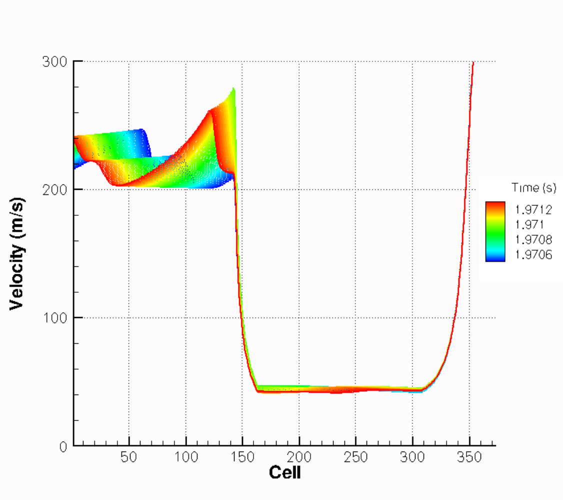

(a) M_{in}=0.7

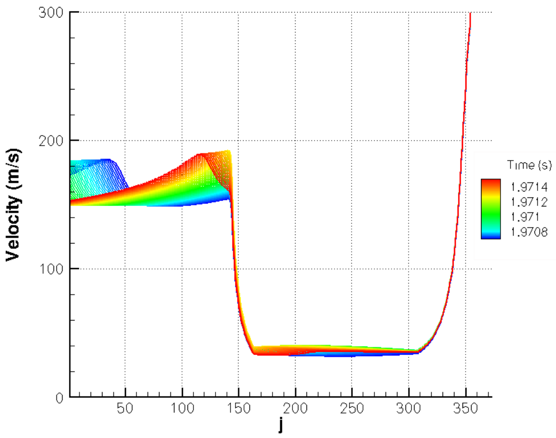

(b) M_{in}=0.55

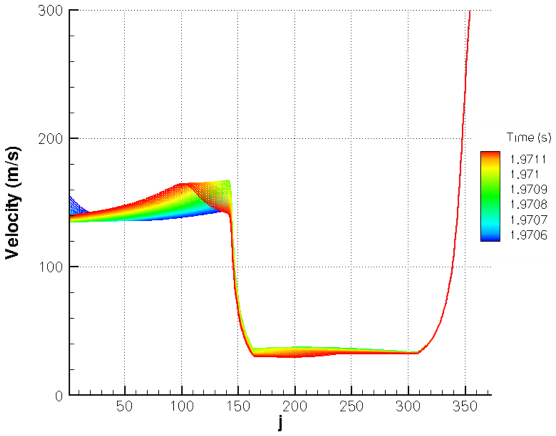

(c) M_{in}=0.44

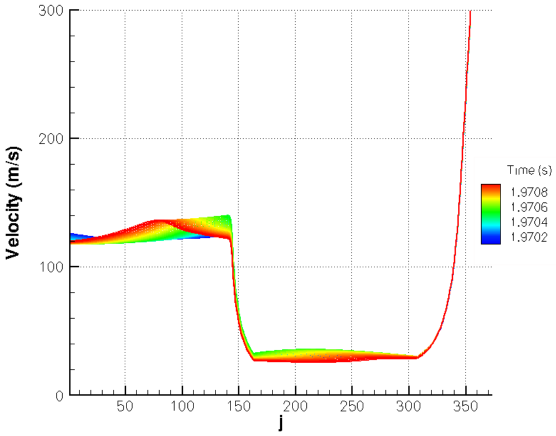

(d) M_{in}=0.38

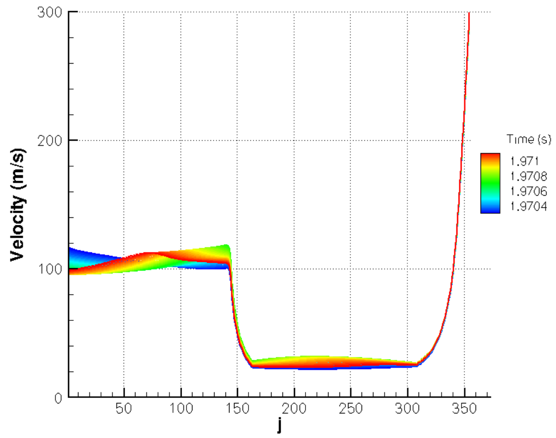

(e) M_{in}=0.32

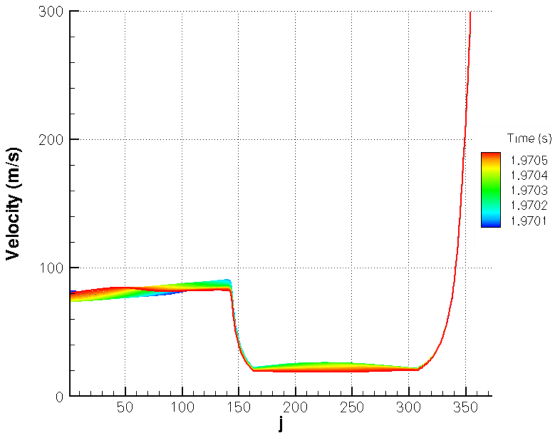

(f) M_{in}=0.25

Figure 10: M_{in} effects - Velocity combustion chamber distribution.

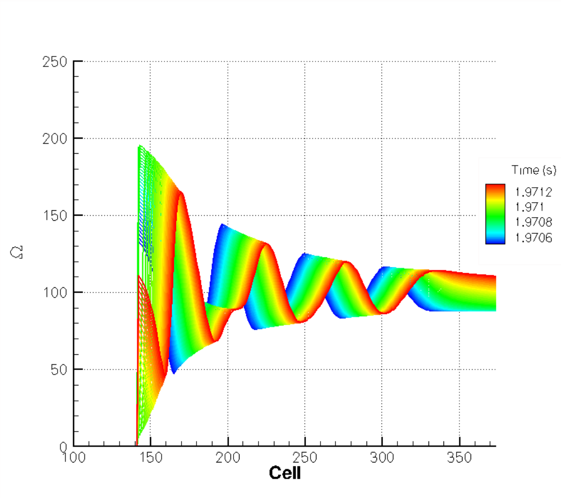

(a) M_{in}=0.7

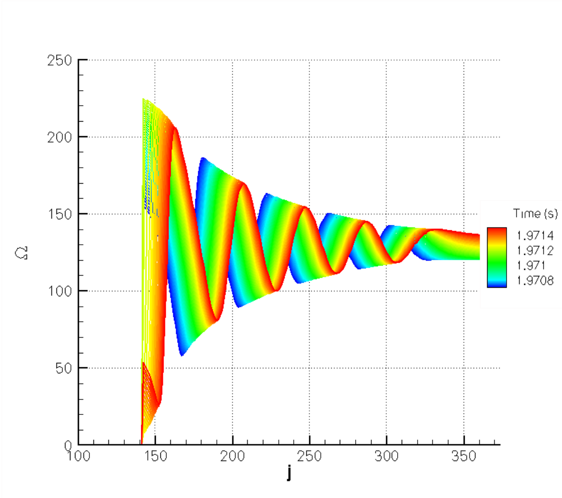

(b) M_{in}=0.55

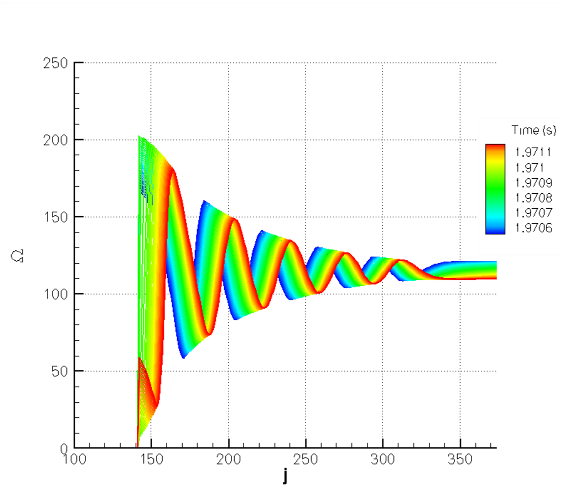

(c) M_{in}=0.44

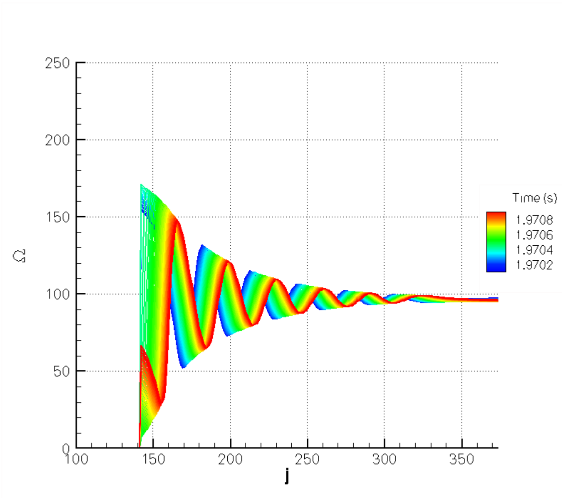

(d) M_{in}=0.38

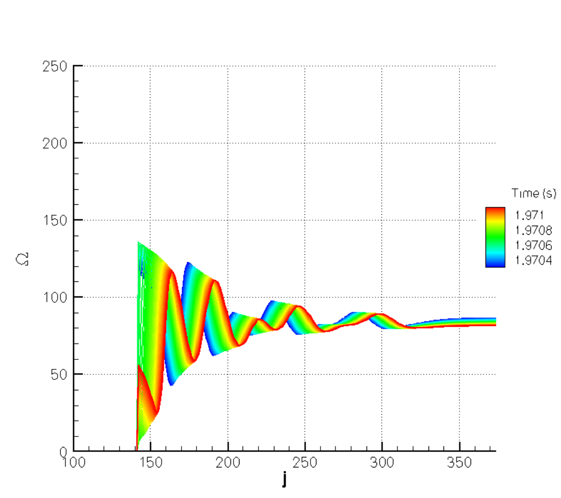

(e) M_{in}=0.32

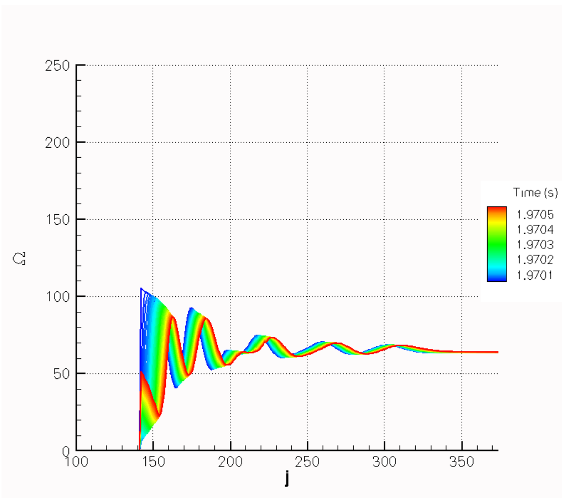

(f) M_{in}=0.25

Figure 11: M_{in} effects - Ω distribution.

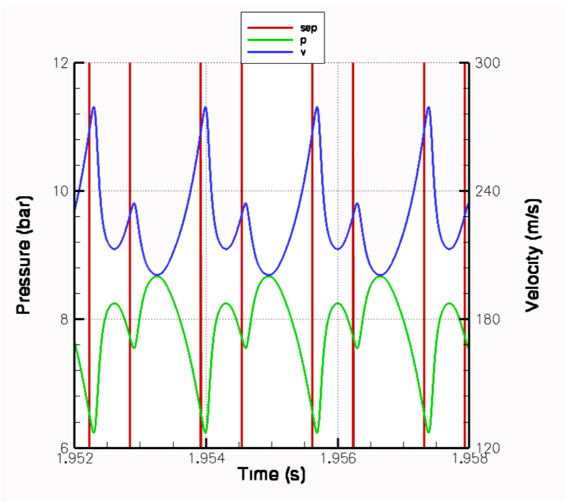

(a) M_{in}=0.7

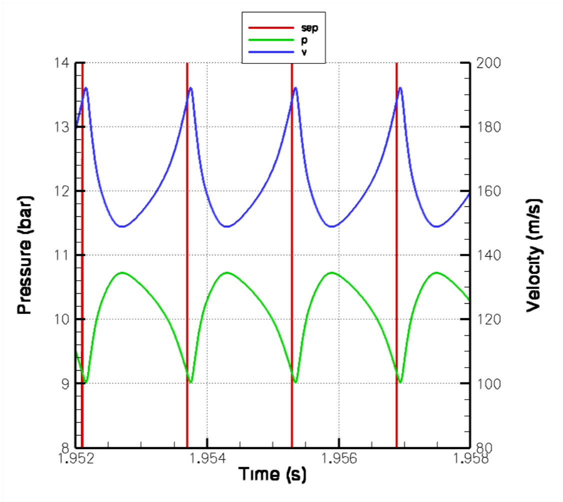

(b) M_{in}=0.55

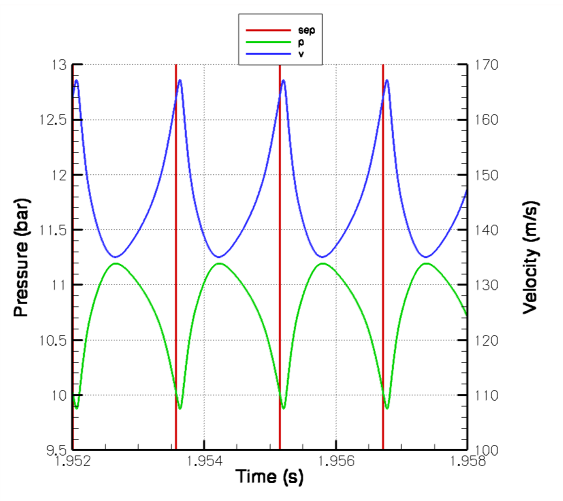

(c) M_{in}=0.44

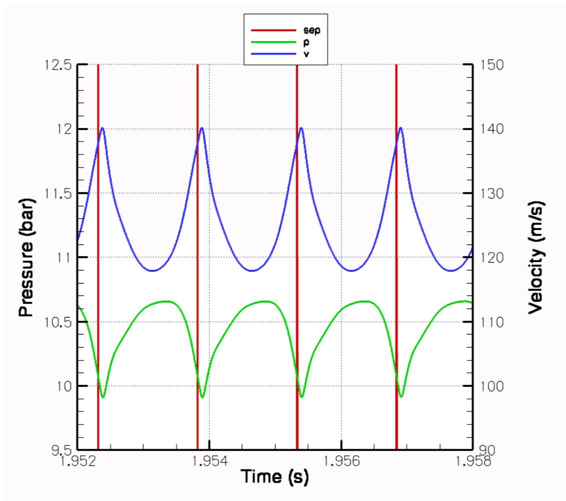

(d) M_{in}=0.38

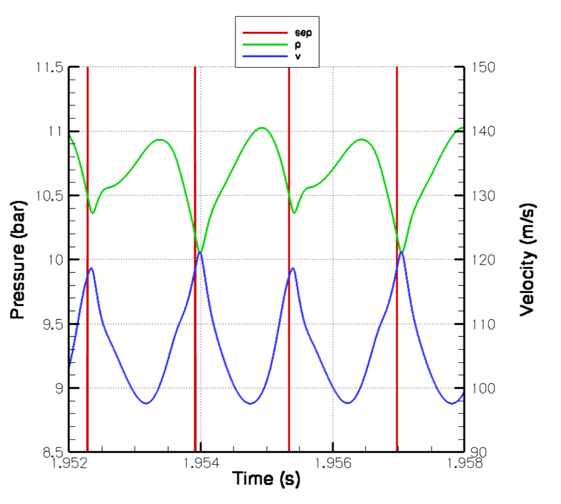

(e) M_{in}=0.32

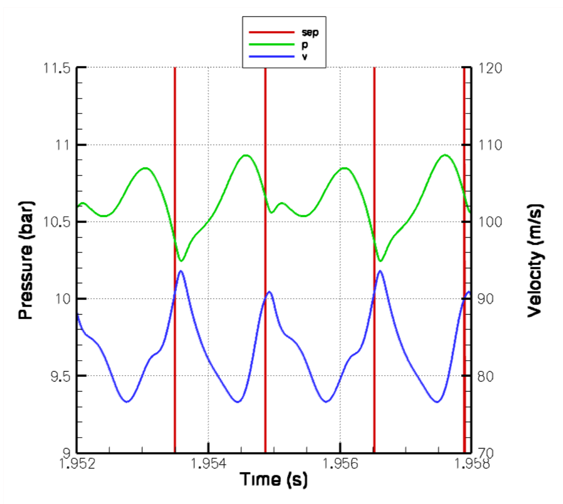

(f) M_{in}=0.25

Figure 12: M_{in} effects - Vortex detachment condition.

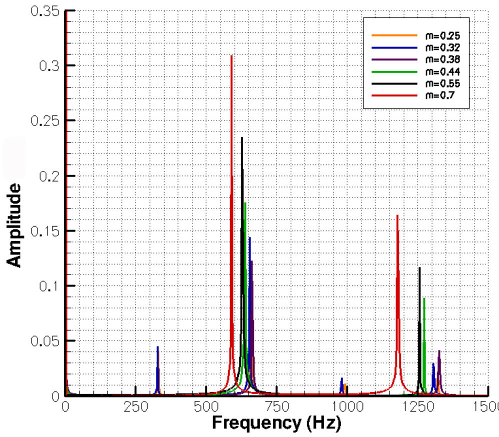

(a) Pressure - Base of the step

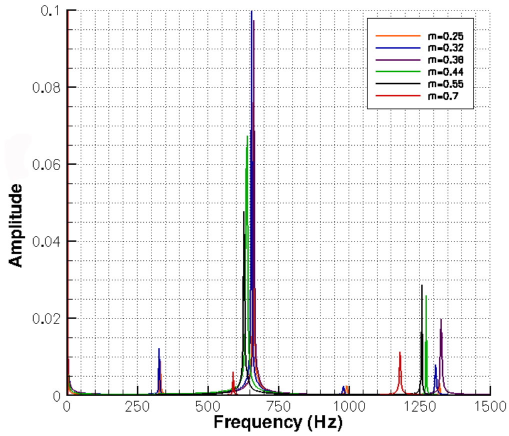

(b) Pressure - Nozzle throat section

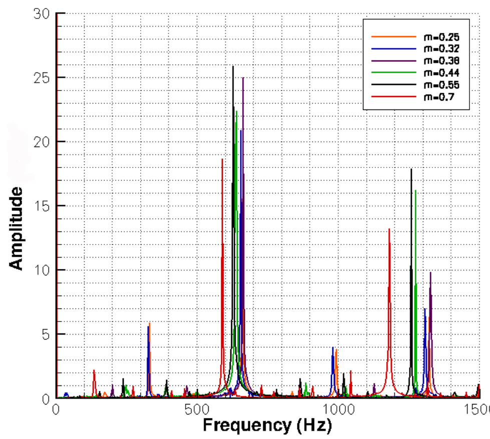

(c) Ω - Step

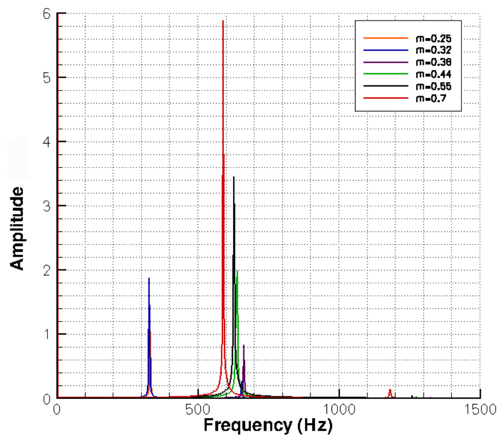

(d) Ω - Nozzle throat section

Figure 13: M_{in} effects - Pressure and Ω spectrum

References

[1] Flatau, A. and Van Moorhem, W., "Prediction of vortex shedding responses in segmented solid rocket motors," *AIAA Paper 90-2073*, 1990.

[2] Scippa, S., Pascal, P., and Zanier, F., "Ariane 5 - MPS - Chamber pressure oscillations full scale firing results analysis and further studies," *AIAA Paper 94-3068*, 1994.

[3] Rossiter, J. E., "The effect of cavities on the buffeting of aircraft," Royal Arircraft Establishment, Technical memo, 1962.

[4] Culick, F. E. C., "Acoustic oscillations in solid propellant rocket chambers," *Astronautica Acta*, Vol. 12, No. 2, 1966.

[5] Flandro, G. A., "Vortex driving mechanism in oscillatory rocket flows," *Journal of Propulsion and Power*, Vol. 2, No. 3, 1986.

[6] Matveev, K. I. and Culick, F. E. C., "A model for combustion instability involving vortex shedding," *Combust. Sci. and Tech.*, Vol. 175, 2003.

[7] Matveev, K. I., "Reduced-oder modeling of vortex-driven excitation of acoustic modes," Acoustic research letters online, 2004.

[8] Menon, S. and Jou, W.-H., "Numerical simulations of oscillatory cold flows in an axisymmetric ramjet combustor," *Journal of Propulsion*, Vol. 6, 1990.

[9] Jou, W. H. and Menon, S., "Modes of oscillation in a nonreacting ramjet combustor flow," *Journal of Propulsion and Power*, Vol. 6, No. 5, 1990.

[10] Ferretti, V., *Numerical simulations of acoustic resonance of Solid Rocket Motor*, Ph.D. thesis, Dipartimento di Ingegneria Aerospaziale e Astronautica, Sapienza, Università di Roma, 2011.

[11] Ferretti, V., Favini, B., Cavallini, E., Serraglia, F., and Di Giacinto, M., "Numerical simulations of acoustic resonance of Solid Rocket Motor," *AIAA-2010-6996*, 2010, 46th AIAA/SAE/ASME/ASEE Joint Propulsion Conference and Exhibit, Nashville, TN, July 25-28, 2010.

[12] Ferretti, V., Favini, B., Cavallini, E., Serraglia, F., and Di Giacinto, M., "Quasi 1-D modeling of SRM aeroacoustics," Space Propulsion Conference, 2010, San Sebastian, Spain.

[13] Cavallini, E., *Modeling and numerical simulation of solid rocket motor internal ballistic*, Ph.D. thesis, Dipartimento di Ingegneria Aerospaziale e Astronautica, Sapienza, Università di Roma, 2009.

[14] Favini, B., Cavallini, E., Ferretti,V., F. Ferraro, Di Giacinto, M., and Serraglia, F., "Gas Mixtures Effects in SRM Ignition Transient," *EUCASS 2011, 4th European Conference for Aerospace Sciences, July 4-8 2011, St Petersburg*, 2011.